AIAA 81-4056

Turbulent Uniform Flow around Cylinders of Finite Length

Dj. Farivar*
University of Tehran, Tehran, Iran

Experimental results are presented which demonstrate the effects of the free end of a circular cylinder on the mean and fluctuating pressures, mean drag force, and the phenomenon of vortex shedding when the cylinder was exposed to uniform flow. The work was carried out at Reynolds number of 0.7×10^5, and turbulence level of 0.9%. The results of the pressure measurements indicated the presence of a suppressed two-dimensional region on the lower part of the cylinder. The functional relationship between the absolute maximum fluctuating pressure coefficient and cylinder length/diameter ratio was obtained. The accuracy of the drag measurements was checked by integrating the pressure profiles, and excellent agreement between the integrated pressure data and the direct measurement was obtained. The vortex shedding measurements suggested the possible existence of three distinct sets of vortex rows with different frequencies. In the lower region, vortex loops were shed with a frequency such that it yielded a Strouhal number appropriate to an infinitely long cylinder.

Nomenclature

$\kappa\chi\lambda C'_{p\max}$	= absolute $C'_{p\max}$
C_D	= $D/\frac{1}{2}\rho U^2 Ld$ = mean drag coefficient
C_p	= $(P-P_\infty)/\frac{1}{2}\rho U^2$ = mean pressure coefficient
C_{Pb}	= mean base pressure coefficient
C'_P	= $P'/\frac{1}{2}\rho U^2$ = fluctuating pressure coefficient
$C'_{P\max}$	= maximum fluctuating pressure coefficient
D	= mean drag force
d	= cylinder diameter
f	= frequency of the vortex shedding
L	= cylinder diameter
LT	= low turbulence
P	= mean surface pressure
P_∞	= freestream static pressure
p'	= corrected fluctuating pressure
Re	= Ud/ν = Reynolds number
S	= $f\cdot d/U$ = Strouhal number
U	= freestream velocity
VLT	= very low turbulence
y	= coordinate along the cylinder axis
ρ	= viscosity of air
θ	= angle measured from front stagnation point
ν	= kinematic viscosity of air
2D	= index indicating two-dimensional
3D	= three-dimensional

Introduction

THE subject of the dynamics of fluid flow around cylinders seems to be constantly in question. The subject has been difficult to understand due to the complicated flow regimes, to which the phenomenon of vortex shedding adds further difficulties. One of the basic problems of the viscous theory, which is still unsolved, is the understanding of the nature of separated flow past bluff bodies at high Reynolds numbers.

A survey of literature indicates relatively few investigations of flow over bluff bodies which attempt to consider end effects. It is the purpose of this paper to present the results of the studies made on the end effects of circular cylinders in a uniform flow. The study involved measurements of mean and fluctuating pressures, mean drag, and Strouhal frequency in low-turbulence (of the order of 1%) uniform flows. The measurements were compared with those obtained here for situations in which the wake flow could be considered two-dimensional and with other results in other literature, as appropriate.

Received Sept. 4, 1979; revision received June 30, 1980.

*Assistant Professor, Civil Engineering Department, College of Engineering.

Related Work

The only published work pertaining to three-dimensional (3D) effects of flows over a circular cylinder in a uniform flow is that of Goettingen,[1] which deals with the drag coefficient C_D. Table 1 provides the values of C_D for various cylinder length/diameter ratios (L/d). In this table $(C_D)_{2D} = 1.17$ is the drag coefficient for an infinitely long cylinder and C_D for the finite-length case.

Apparatus

Wind Tunnel

The experiments were conducted in the University of Pennsylvania low-speed, single-return, closed-circuit wind tunnel with a velocity range of 0.61-61 m/s (2-200 ft/s). With two screens in the settling chamber, the longitudinal component of turbulence intensity was 0.4%. The flow with this turbulence level is designated as very-low-turbulence (VLT) flow in this presentation. An array of equally spaced rods at the entrance to the working section produced a turbulence level of 0.9%, and this flow condition is denoted low-turbulence (LT) flow. The measurements of the velocity in the test section were achieved by means of a pitot-static tube connected to a micromanometer capable of indicating pressures as low as 0.0025 cm (0.001 in.) of water column.

Pressure Measurement Apparatus

The test model consisted of a circular cross-section brass tube of 5.08 cm (2.0 in.) o.d. and was made in modular form such that different sections could be mated smoothly. The 20 pressure taps provided along a generator of the model were positioned such that the taps were closely separated near the top of the model, and the distance between two adjacent taps were increased as the bottom was approached. This gave the advantage that when the model was retracted to the minimum length to diameter ratio of 2.78 considered here, there were still 11 taps exposed to the flow. Pressure taps were connected by vinyl tubing to a 48-port pressure switch housed within the model, and connected to a pressure transducer with a pressure range of ±15.24 cm (±6.0 in.) of the water column.

The model was placed on a turntable anchored rigidly to the laboratory floor under the test section. This way the model could be lowered and raised to expose, through a sufficiently large hole in the tunnel floor, the desired length to the airflow, and meanwhile it could be turned to measure the pressure

Table 1 Drag coefficient for finite-length circular cylinder in uniform incident flow[1]

	L/d							
	1.00	1.98	2.96	5.00	10.0	20.0	40.0	∞
$C_D/(C_D)_{2D}$	0.53	0.57	0.62	0.62	0.68	0.76	0.82	1.00
C_D	0.62	0.67	0.73	0.72	0.80	0.89	1.06	1.17

along the desired model generator. To avoid flow entrainment through the hole, a flexible boot configuration was provided using thin household plastic wrap which did not exert any significant damping effect on the model.

Force Measurement Apparatus

The model designed for the measurement of the drag was made of very light coarse foam covered with thin balsa wood. The model was sanded smooth and then sprayed with epoxy paint, yielding a total resultant weight of little less than 56 g (2.0 oz).

The drag measurement apparatus consisted of two flexural steel plates integrally machined with disks at each end, and was equipped with four electrical strain gages which were connected in such a form that a four-active-arm bridge was formed. The bridge output was connected to a strain indicator and calibrated, so that the system directly measured the true force.

Hot-Film Anemometry

Turbulence, velocity, and Strouhal frequency measurements were made with a TSI constant temperature hot-film sensor connected to a linearized research anemometer having a maximum frequency response capability of 200 KHz. The hot-film sensor could be traversed with the application of a DISA linear traversing mechanism coupled with external stepper motor and sweep drive unit.

Associated Equipment

Where necessary, the pressure transducer and the force measurement apparatus signals were displayed on a Tektronix dual-beam oscilloscope, equipped with a Tektronix camera system to provide photographic records for subsequent analysis, as appropriate. A TSI true rms/dc/mean-square digital voltmeter was used to record the dc level or root mean square (rms) of the pressure signals.

Experimental Procedure and Results

A series of experiments, for both VLT and LT uniform flows, was conducted to determine the following: 1) the distribution of the mean pressure over a circular cylinder with end effect, 2) the distribution of the rms value of the fluctuating pressure over the cylinder, 3) the mean drag force, and 4) the frequency of the vortex shedding.

The results of the pressure measurements indicated that the mean pressure coefficient C_P was, at most, only a very weak function of Reynolds number Re in the range of $0.2\times10^5 < Re < 1.3\times10^5$. Also, a comparison of the measurements revealed that the different turbulence levels produced only negligible differences in the pressure coefficients. Therefore, all the measurements were carried out at one Reynolds number, namely $Re=0.7\times10^5$, and a turbulence level of 0.90%.

Viscous effects in relatively long tubing connecting a pressure tap on the model surface to a port of the pressure switch introduced amplitude and phase changes in the signals. Amplification rather than attenuation could occur if the fluctuating pressure happened to harmonize with the Helmholtz resonator frequency of the cavity representing the volume of the connecting tube and the internal passages of the pressure switch. The extent of these effects was determined through the use of a calibration device. The device provided a calibration range to almost the second harmonic of the highest estimated fundamental vortex shedding frequency.

Experiments were conducted for finite model length to diameter ratios, L/d = 2.78, 5.0, 7.5, 10, 11, and 12.5, and in each case a complete mean and fluctuating pressure survey, as well as drag measurement, were made. The case with L/d = 15 corresponded to the case in which the model spanned the tunnel and, therefore, represented the infinite length configuration.

Figures 1 and 2 illustrate the variation of C_P and C_P' with θ for models of L/d = 5 and 10. In these figures y represents the height measured from the base of the model. Vortex shedding was detected with the oscilloscope connected to the pressure transducer output and the Strouhal frequency f was measured from photographs of the signals. A sample of such photograph is shown in Fig. 3.

The oscilloscope displays of the pressure signals were readable for models with $L/d > 7.5$. The signals for shorter models were very random, and no definite frequencies could be determined, especially in the region of the top of the model where the three-dimensional effects were most significant. Figure 4 illustrates the Strouhal number S vs height for several values of L/d. To check the validity of these results the frequency of the vortex shedding was also measured using the hot-film anemometer. The hot-film sensor was traversed a short distance in the wake (of the order of one cylinder diameter) in the streamwise direction as well as along the

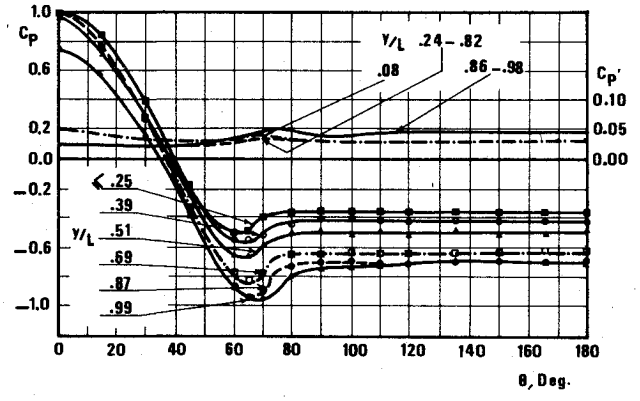

Fig. 1 Mean and fluctuating pressure distribution on cylinder, $L/d=5.0$.

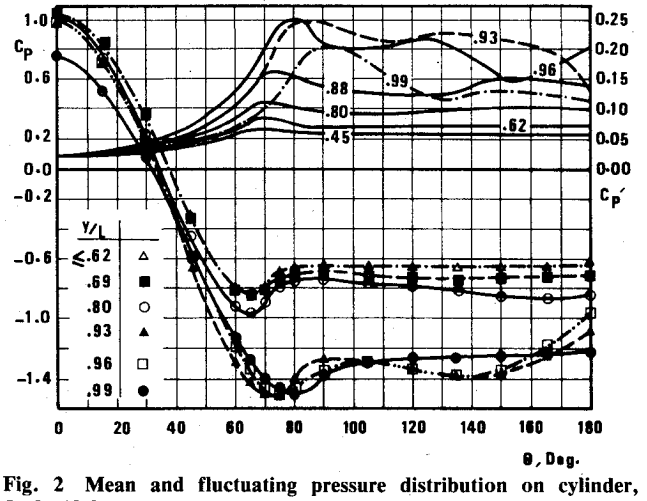

Fig. 2 Mean and fluctuating pressure distribution on cylinder, $L/d=10.0$.

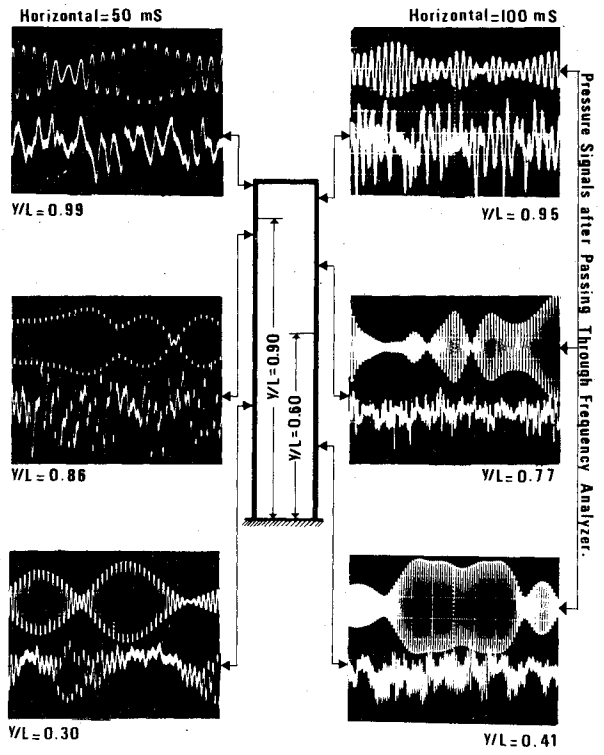

Fig. 3 Pressure signals at six points on model, $L/d = 11.0$.

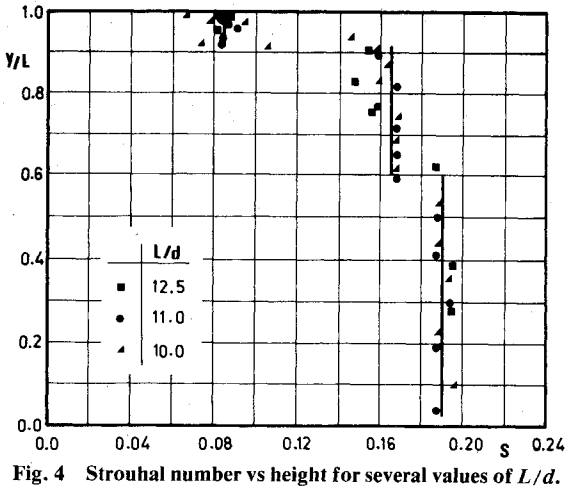

Fig. 4 Strouhal number vs height for several values of L/d.

model. The output of the hot film was displayed on the oscilloscope and the results were photographed, samples of which are shown in Fig. 5. As can be seen, both procedures indicate changes of Strouhal frequencies along the model.

Discussion of Results

Pressure Analysis

The distribution of C_P around the cylinder for various values of y/L with $L/d = 12.5$ showed that for 80 deg $\leq \theta \leq 280$ deg, the base pressure coefficient, C_{Pb}, was essentially constant for each y/L, with approximately the same value of C_{Pb} occurring for the range $0.39 \leq y/L \leq 0.81$. For $y/L < 0.39$ it appeared that the change in C_{Pb} with y/L was due to the presence of the tunnel floor boundary layer. This variation was also observed in the case of a cylinder spanning the tunnel. It was concluded that C_{Pb} was independent of the ratio y/L for $y/L \leq 0.81$. This phenomenon was also observed for other values of L/d but with different limiting values of y/L (Figs. 1 and 2). The behavior was explained as follows.

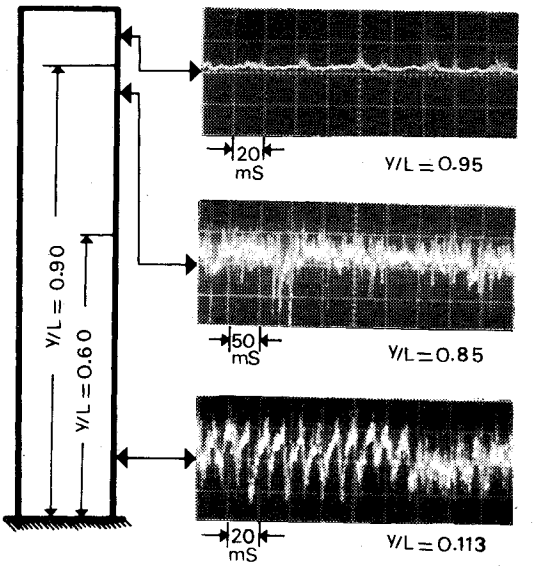

Fig. 5 Hot-wire anemometer signals when placed in wake of model, $L/d = 10.0$.

The region in which the pressure coefficient was a 3D function did not extend all the way down to the base of the model, but rather it diminished as y/L decreased. Therefore, on the lower portion of the model, the pressure appeared as though due to a suppressed two-dimensional wake flow with C_P having a value higher than that for the classical (or ideal) case. Designating by $(y/d)_{2D}$ the length over which the C_{Pb} was constant, it was conjectured that C_{Pb} and $(y/d)_{2D}$ should be a function of L/d, the only parameter to be varied. It was found that the $(y/d)_{2D}$ and C_{Pb} results could be reasonably well fitted by:

$$(y/d)_{2D} = 0.097(L/d)^{1.78} \tag{1a}$$

$$(C_{Pb})_{2D} = 0.78(y/L)_{2D} - 0.15 \tag{1b}$$

as shown in Figs. 6a and 6b, where the straight line in the second equation extends from $(y/L)_{2D} = 0.27$ to 0.82, corresponding to $L/d = 13$, the maximum value before significant interference from the tunnel roof boundary layer was encountered. The next available point was the limiting case of $L/d \to \infty$ for which $(y/L)_{2D} = 1.0$ and $C_{Pb} = -1.13$, and it would appear that the straight line should approach this point asymptotically. To include the upper limit for large values of L/d, Eq. (1b) may be written in the following form:

$$\frac{(C_{Pb})_{2D} + 0.15}{-0.78(y/L)_{2D}} = 1.0 + F\{(y/L)_{2D}\} \tag{2}$$

where

$$F\{(y/L)_{2D}\} = -0.45 \text{ for } (y/L)_{2D} = 1.0$$

and

$$F\{(y/L)_{2D}\} \ll 1.0 \text{ for } (y/L)_{2D} \leq 0.8$$

For $0.8 < (y/L)_{2D} < 1.0$, F represents a function which approaches 0.45 asymptotically as $(y/L)_{2D}$ approaches unity.

The pressure distributions over the front portion of the model in suppressed two-dimensional flow for $\theta \leq 75$ deg are shown in Fig. 7 for various values of L/d together with the fully two-dimensional wake flow case. The shapes of the curves suggested a sinusoidal relation between C_P and θ, with stagnation pressure coefficient equal to 1.0 regardless of L/d, and a minimum C_P occurring near $\theta = 64$ deg $= 1.11$ rad. The

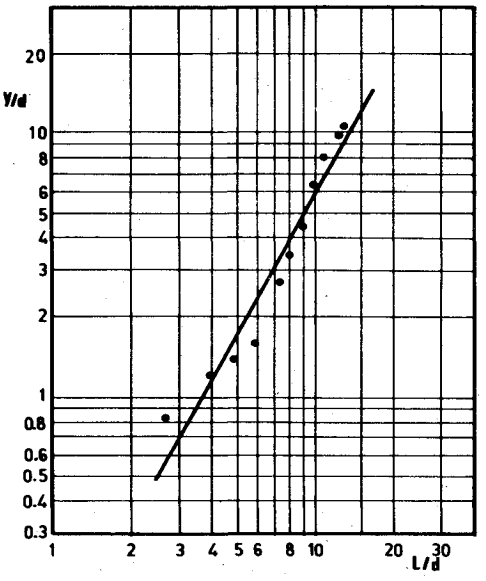

Fig. 6a Aspect ratio y/d vs L/d.

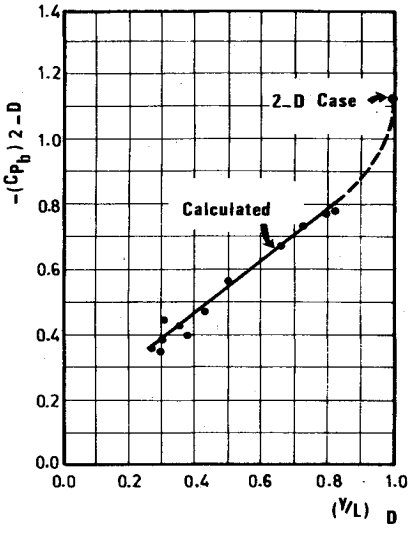

Fig. 6b Base pressure coefficient at different heights over which wake flow is two-dimensional.

functional relationship between C_P, θ, and L/d was found to be

$$C_P = a_1 \cos(2.842\theta) + a_2 \tag{3}$$

where

$$a_1 = -0.09 \sin\{0.483(L/d - 1.75)\} + 0.84 \tag{4a}$$

and

$$a_2 = 1.0 - a_1 \tag{4b}$$

Figure 7 compares the distribution of C_P *for* $\theta \leq 75$ deg over the suppressed two-dimensional portion as found experimentally and by Eq. (3). The above equations do not represent the limiting case when $L/d \to \infty$, and therefore a separate analysis for the infinitely long cylinder led to the following:

$$C_P = 1.1 \cos(2.57\theta) - 1.0, \qquad \theta \leq 1.36 \text{rad} = 78 \text{ deg} \tag{5a}$$

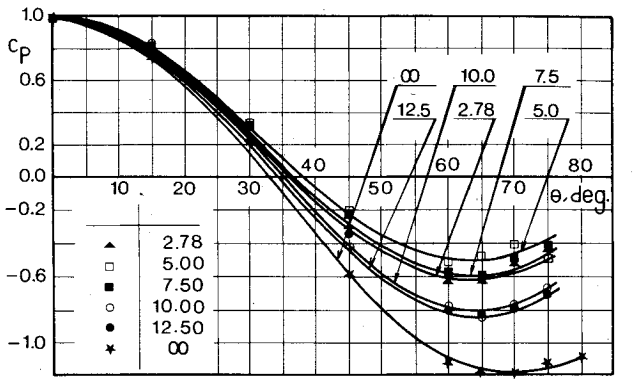

Fig. 7 Calculated and experimentally obtained C_P on suppressed two-dimensional part of cylinder.

and

$$C_{Pb} = -1.13, \qquad \theta \geq 78 \text{ deg} \tag{5b}$$

As might be expected there is a close resemblance between C_P distribution in potential flow ($C_P = 2\cos(2\theta) - 1$), and Eqs. (3) and (5). For potential flow, i.e., two-dimensional and infinite Re, the minimum C_P occurred at $\theta = 90$ deg and its magnitude was -3.0, but, for $Re = 0.7 \times 10^5$, the location of minimum C_P moved upstream to $\theta = 70$ deg and its value increased to -1.3. At the same Re when the model was retracted, the minimum C_P over the lower part (in the suppressed two-dimensional region) increased further and its location moved even further upstream. A collection of the results of different authors for two-dimensional wake flow behind a circular cylinder at different Re showed that, as Reynolds number decreased, the minimum C_P increased and the location of this minimum moved upstream.[2-4] Analogous to this, C_P for the lower part of the model behaved as though the flow were two-dimensional with a lower Re, and as L/d increased this Reynolds number decreased. For this reason, the flow around the lower part of the model was called "suppressed two-dimensional" earlier in this presentation.

Fluctuating Pressure Analysis

Examination of the distributions of fluctuating pressure coefficient C_P readily indicated a peak value around $\theta = 75$ deg in almost every case (see Fig. 2). Achenbach[5] showed that the point of separation of the flow from cylinder for the case of subcritical flow ($Re = 10^5$) occurred at $\theta = 78$ deg. Son and Hanrathy[6] observed that at this Re the flow separated from the cylinder at $\theta = 77$ deg and that it coincided, within the experimental accuracy, with the first peak in the distribution of C_P'. Batham[7] concluded that the maximum C_P' at the separation point may be caused by intermittent collapse of the vortices. The foregoing discussion strongly suggests that the maximum fluctuating pressure coefficient occurs at the point of separation and is indicated by a peak in the C_P' distribution curves. Measurements showed that C_P' was not constant along the model length, even in the case in which the cylinder spanned the tunnel as Fig. 8 illustrates. It is seen that C_P' was fairly symmetrical with respect to the model median and the maximum value occurred near $\theta = 75$ deg, with the minimum value occurring along the stagnation generator. For a constant angle θ, C_P' was maximum at the cylinder median, and the absolute maximum occurred at $y/L = 0.5$ and $\theta = 75$ deg. Figure 9 indicates that the wake flow cannot be treated as two-dimensional with respect to the fluctuating pressure.

The maximum fluctuating pressure at a particular height $C'_{P\,\max}$ is plotted in Fig. 9 vs y/L for various model lengths. It is seen that the lower portion of the model experienced pressure fluctuations which did not vary significantly with y/L, but pronounced variations were observed as the tip was

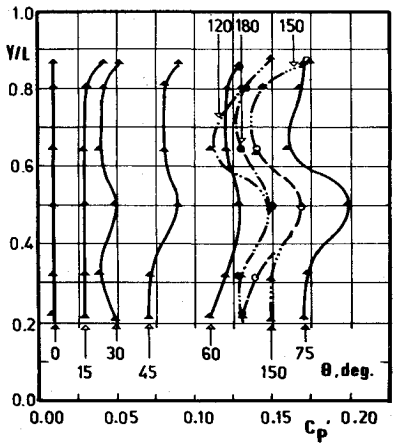

Fig. 8 Distribution of C_P' along cylinder's generators in two-dimensional wake flow.

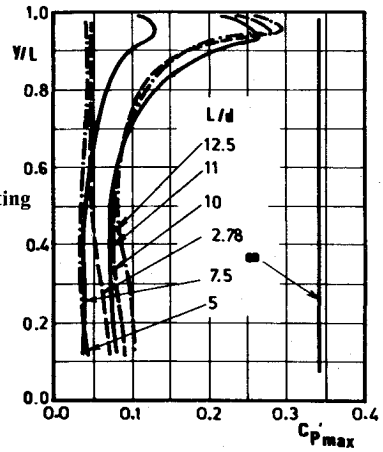

Fig. 9 Maximum fluctuating pressure coefficients vs y/L.

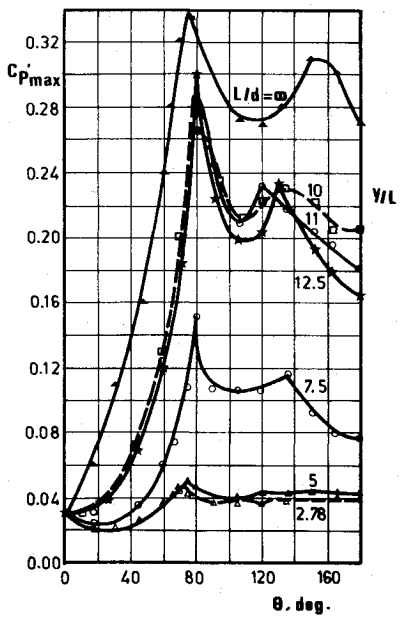

Fig. 10 Distribution of maximum fluctuating pressure coefficient around cylinder.

approached. The fluctuations peaked near the cylinder tip, especially for taller models, and decreased to match the fluctuating pressures on the cylinder's roof, which were of the order $C_P' = 0.03$ at $\theta = 75$ deg and independent of the length. Hence the C_P' gradient would be larger near the tip of a more slender model.

The $C_{P\max}'$ peaks in Fig. 9 occurred at $y/L = 0.95 \pm 2\%$, and the distribution of the pressure fluctuations at this height is shown on Fig. 10. For different values of L/d, the first peak of each curve corresponds to that of Fig. 9 and is the absolute

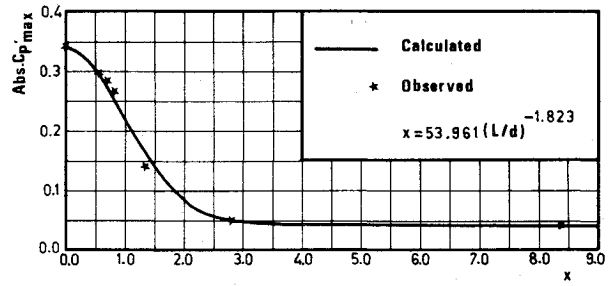

Fig. 11 abs$C_{P\max}'$ vs x for cylinders in uniform flow.

Table 2 Calculated and observed values of absolute maximum pressure fluctuations

L/d	x	$f(x)$	abs$C_{P\max}'$ Calculated	abs$C_{P\max}'$ Observed
∞	0.000	0.399	0.340	0.340
12.50	0.540	0.345	0.300	0.300
11.00	0.682	0.317	0.279	0.286
10.00	0.811	0.288	0.258	0.267
7.50	1.370	0.156	0.160	0.140
5.00	2.870	0.007	0.050	0.050
2.78	8.370	0.000	0.045	0.045

maximum pressure fluctuation on the cylindrical model. This maximum value was designated by abs$C_{P\max}'$. An examination of Fig. 10 indicates that abs$C_{P\max}'$ occurred at/or about $\theta = 80$ deg. Curve fitting of the data indicated that

$$\text{abs}C_{P\max}' = 0.739 f(x) + 0.045 \tag{6}$$

where $f(x)$ is the function for the probability density of a standardized Gaussian random variable of the form

$$f(x) = (1/\sqrt{2\pi}) e^{-\frac{1}{2}x^2} \tag{7}$$

and

$$x = 53.961 (L/d)^{-1.823} \tag{8}$$

Table 2 provides a comparison between the values of abs$C_{P\max}'$ found by experiment and by Eqs. (6-8). It is seen that Eq. (8) covers all values of L/d, including the limiting case of an infinitely long cylinder. Figure 11 illustrates Table 2 graphically.

Mean Drag Force

The mean drag forces experienced by the cylinders of various L/d were obtained by different methods and the results were compared. At $Re = 0.7 \times 10^5$ the direct measurement of the drag force, by means of the force measurement device obtained for the model spanning the tunnel in both LT and VLT flows, yielded mean drag coefficients C_D of 1.22 and 1.17, respectively. The drag coefficient obtained by integrating the pressure field along the model height was found to be $C_D = 1.15$ which shows a close agreement with that found by direct measurement. C_D for this situation was also calculated through the use of Eqs. (5) on the assumption that there was no significant variation of C_P along the model span. It was found that $C_P = 1.14$ which is comparable with the above values.

The models not spanning the tunnel, C_D was found by both the direct measurement and the integration of the measured pressures around and along the model. The drag coefficient would be:

$$C_D = \tfrac{1}{2} \sum_j \sum_i C_{P_i} \cos\theta_i \, \Delta(y/L)_j \, \Delta\theta_i \tag{9}$$

Table 3 Drag coefficients for finite length cylinders in uniform flow

	$C_D/(C_D$ for infinite length cylinder)			
		Present study, $Re = 0.70 \times 10^5$		
	Goettingen[1]	VLT flow	LT flow	
L/d	$Re = 0.88 \times 10^5$	DM[a]	DM[a]	PI[b]
∞	1.00	1.00	1.00	1.00
40	0.82	–[c]	–	–
20	0.76	–	–	–
12.5	–	0.73	0.78	0.75
11	–	–	0.76	–
10	0.68	0.67	0.72	0.73
9	–	–	0.67	–
7.5	–	0.57	0.58	0.59
6	–	–	0.55	–
5	0.62	0.52	0.55	0.50
4	–	–	0.52	–
3	–	–	0.52	–
2.96	0.62	–	–	–
2.78	–	0.52	0.51	0.24
1.98	0.57	–	–	–
1.00	0.53	–	–	–

[a] Direct measurement. [b] Pressure integration. [c] Not measured.

The values of drag coefficients were calculated using Eq. (9) and the pressure data. The results of both procedures are shown in Table 3. As the results show, the effect of the free end of the cylinder on the profile drag depends on the ratio of L/d, and the drag decreased as L/d decreased. This was to be expected because, when the cylinder is of finite length, a departure of the flow from the two-dimensional pattern occurs toward the free end, causing the wake pressure to increase around the base of the cylinder (suppressed flow). This increase in the wake pressure yields a lower drag. As was seen in the preceding sections, the rate of increase in the wake pressure was more for smaller L/d, and therefore a shorter model would experience less drag.

Experiments showed that for the same L/d and Re, the addition of 0.5% turbulence to the freestream turbulence level did not measurably change the total force experienced by the cylinder. This indicates that the separation point did not move toward the rear, as it did when the change in turbulence level was high.[7]

The agreement between measured and calculated drag coefficients is noticeable. The values found by integration of pressure data seem generally lower than the direct measured values, and this was attributed to the fact that the former did not include the skin friction. According to Thom[8] the skin friction drag coefficient varies as $4Re^{-\frac{1}{2}}$, which shows that at high Re the effect of skin friction is negligible. For a short model the portion of the length in the boundary layer was comparable with the total length of the model. Due to the low velocity and therefore low Re in the tunnel floor boundary layer, the actual pressure measured around the model was low and the skin friction drag was high. Since the pressure coefficient was based upon the freestream core velocity, and not local velocity, the C_P thus obtained was lower than the true C_P value which yielded a lower drag coefficient.

Discussion of the Frequency of Vortex Shedding

For the cylinder not spanning the tunnel it was shown that the model could be divided into three distinct parts with respect to the frequency of the vortex shedding associated with each part: a small top region characterized by low-frequency vortex shedding, a middle region characterized by higher frequency (still lower than that for a classical wake flow), and a lower region characterized by a Strouhal number equal to that for a classical wake flow. This is shown in Fig. 4, and the lower region confirms the existence of the suppressed two-dimensional region. No detailed studies were made of the wake, but a possible explanation follows.

Roshko[9] conducted a series of experiments with a splitter plate placed parallel to the stream and in the wake of a circular cylinder, and observed a decrease in the Strouhal number as he moved the plate away from the cylinder. Gerrard[10] gave an explanation for this phenomenon in terms of the size of the formation region. He and Roshko[11] observed that as the size of the formation region was increased, the frequency of the vortex shedding decreased. Hence, the decrease in the Strouhal number observed by Roshko was due to a flow regime in which the formation region was lengthened so as to include the plate in its interior. In effect, the splitter plate provides a seat for the elongating vortex pair so that they can remain stably in position at a higher Re than they would without the plate. Hence, when periodic detachment starts, the vortices are stronger and less frequent (giving the observed lower Strouhal number) than in the case with no plate.

In the case of a cylinder with one end free in a uniform stream, the flow over the top of the cylinder deflects and enters the wake region around the top. This entrainment causes a blockage in the wake preventing the interaction between the vortices and, hence, the formation region elongates in order to provide sufficient surface for the diffusion of the vorticity which is being continuously produced. This phenomenon will delay the action of the vortex shedding around the free end of the cylinder, but cannot explain the occurrence of the multiple frequencies along the span of the cylinder.

To provide additional information, tests were performed of the vortex shedding frequency by means of hot-wire anemometry. In traversing the hot film along the model, the first sign of vortex shedding behind the cylinder was detected at $y/L = 1.0$ and no sign of vortices was observed at a height of $y/L > 1$, at least for 1.5 diameters downstream of the cylinder axis. This suggests that the vortex lines bend at $y/L = 1$ and terminate either on themselves (as closed loops) or on a solid boundary, without any other possible alternative. These vortex lines cannot terminate on the tunnel ceiling, since for a very short model or for the case of one boundary at the cylinder base, there is no reason for the existence of vorticity at $y \gg L$. Aside from the separated boundary-layer vorticity, there is also the cylinder tip region vorticity produced by the low pressure in the wake, thus overtopping with its axis in a direction perpendicular both to model axis and to the flow direction. This indicates that an open vortex loop is formed which consists of the separated boundary-layer vorticities, similar to those in an infinite length cylinder wake flow, with staggered positions as in a Karman vortex street and the roof region vorticity.

The jumps in the frequency at two locations along the cylinder indicate the existence of a surface of discontinuity at these locations and, therefore, the existence of isolated vortex loops with different detachment frequencies. The one possible configuration of these vortex loops is rows of rings. Levy and Forsdyke[12] have proved that this configuration is unstable and as a result, as Rosenhead (see Ref. 12) has suggested, the only stable configuration would be sequences of irregularly shaped vortex loops.

The system of three rows of irregularly shaped vortex loops, with different detachment frequencies, could explain the three frequencies observed on the pressure transducer and hot-wire anemometer signals.

Conclusions

Based upon the experimental results the following remarks can be made concerning the end effect of a circular cylinder tested in a uniform flow:

1) As far as pressure field is concerned, two distinct areas can be distinguished. The first is a suppressed two-dimensional flow region extending from the cylinder base to a height equal to $(y/d)_{2D}$. In this region the base pressure coefficient is independent of height and, for the same θ, C_P is

higher than that for a cylinder spanning the tunnel. C_P for this portion follows a sinusoidal relationship, with θ and L/d being variables. The second area is a three-dimensional wake flow regime over the top portion extending from $(y/d)_{2D}$ to the cylinder tip, with the pressure being a function of y/L.

2) Generally at any height, the fluctuating pressure peaks at $\theta = 75$ deg. The absolute maximum fluctuations occurs at $y/L \simeq 0.95$, with a value depending on L/d. The functional relationship between these maximums and $x = F(L/d)$ resembles the function for the probability density of a standardized Gaussian random variable.

3) For a finite length, projecting cylinder the effect of the free end is to decrease the mean drag coefficient as L/d is decreased.

4) A finite-length projecting cylinder in uniform flow sheds three rows of irregularly shaped vortex loops with frequencies independent of L/d and which increase as y/d is decreased. The vortex shedding frequency in the lower region yields a Strouhal number equal to that for an infinitely long cylinder. The change in frequencies is attributed to the cylinder tip region vorticity.

References

[1] Goldstein, S., ed., *Modern Developments in Fluid Dynamics,* Vol. 2, Dover Publications, Inc., New York, 1965, p. 439.

[2] Roshko, A., "A New Hodograph for Free-Stream Theory," NACA TN 3168, 1954.

[3] Sarpkaya, T., Rainey, P. G., and Kell, R. E., "Flow of Dilute Polymer Solutions About Circular Cylinders," *Journal of Fluid Mechanics,* Vol. 57, Pt. 1, 1973, pp. 178-208.

[4] Thom, A., "Flow Past Circular Cylinders at Low Speed," *Proceedings of Royal Society of London,* Series A, Vol. 141, 1933, pp. 651-668.

[5] Achenbach, E., "Distribution of Local Pressure and Skin Friction Around a Circular Cylinder in Cross-Flow up to Re = 5×10^5," *Journal of Fluid Mechanics,* Vol. 34, Pt. 4, 1968, pp. 625-639.

[6] Son, J. S. and Hanrathy, T. J., "Numerical Solution for the Flow Around a Cylinder at Re = 40, 200, and 500," *Journal of Fluid Mechanics,* Vol. 35, Pt. 2, 1969, pp. 369-386.

[7] Batham, J. P., "Pressure Distribution on Circular Cylinder at Critical Reynolds Number," *Journal of Fluid Mechanics,* Vol. 57, Pt. 2, 1973, pp. 209-228.

[8] Goldstein, S., ed., *Modern Developments in Fluid Dynamics,* Vol. 2, Dover Publications, Inc., New York, 1965, p. 425.

[9] Roshko, A., "On the Drag and Shedding Frequency of Two-Dimensional Bluff Bodies," NACA TN 3164, 1959.

[10] Gerrard, J. H., "The Mechanics of Formation Region of Vortices Behind Bluff Bodies," *Journal of Fluid Mechanics,* Vol. 25, Pt. 2, 1966, pp. 401-413.

[11] Roshko, A., "On the Development of Turbulent Wakes for Vortex Stream," NACA Rept. 1191, 1954.

[12] Goldstein, S., ed., *Modern Developments in Fluid Dynamics,* Vol. 2, Dover Publications, Inc., New York, 1965, p. 578.